



MUNDFAB

This project has received funding from the European Union's Horizon 2020 research and innovation programme under grant agreement No 871813.

ICT Project No 871813
MUNDFAB
Modeling Unconventional Nanoscaled
Device FABrication

**D3.1: Review of experimental and model state
of the art**

B. Sklenard (CEA-Leti), Anna Johnsson (Fraunhofer)
and A. La Magna (CNR-IMM)

03/07/2020



Quality management

This deliverable was reviewed by:

Denis Rideau (STMicroelectronics)

Emmanuel Scheid (CNRS-LAAS)

Contents

Abstract.....	3
1 Experimental review	3
1.1 Full-sheet epitaxy	3
1.1.1 Si growth	3
1.1.2 SiGe growth.....	5
1.1.3 Etching	7
1.1.4 In-situ doping: SiGe:B and Si:P.....	8
1.2 Patterned substrates	9
2 Modeling review	10
2.1 Simulations of full-sheet epitaxy with Sentaurus Process	10
2.1.1 Simulation of silicon epitaxial growth.....	11
2.1.2 Simulation of epitaxial growth of SiGe.....	15
2.2 Epitaxy simulation with MulSKIPS.....	17
Conclusions.....	19
References.....	20

Abstract

This deliverable reviews the state of the art of epitaxy process of Si and SiGe films by CVD (Chemical Vapor Deposition) from an experimental and modeling perspective. The most advanced LKMC (Lattice Kinetic Monte Carlo) CVD epitaxy model implemented in Sentaurus Process is benchmarked against experimental data. In addition, the LKMC model implemented in MulSKIPS to simulate PVD (Physical Vapor Deposition) epitaxy is presented and possible extensions for the simulation of CVD epitaxy are presented.

1 Experimental review

There are two main epitaxy techniques to grow crystalline layers:

- Molecular Beam Epitaxy (MBE)
- Chemical Vapor Depositions (CVD)

Among them, the CVD epitaxy is the method of choice to produce high quality layers in many industrial applications such as Raised Source Drain (RSD) regions in CMOS transistors or for the fabrication of Heterojunction Bipolar Transistors (HBTs). In this report, we focus on reduce-pressure CVD (RP-CVD)¹, which is the main technique used in the semiconductor industry to grow Si based structures.

In RP-CVD, volatile precursors are delivered using a carrier gas (usually H₂) and react with the substrate surface in an epitaxy chamber at temperatures between 350°C and 1200°C. The growth rate depends on different process parameters such as the nature of the precursors and their mass flows, the temperature, the pressure, the substrate orientation and the nature of carrier gas. In Section 1.1, the influence of these parameters will be reviewed in the case of epitaxial layers grown on blanket wafers. In many technological applications, Selective Epitaxial Growth (SEG) on patterned structures is of paramount importance and will be reviewed in Section 1.2. It is important to note that before any epitaxy, a substrate surface preparation is mandatory in order to start the growth process on a clean surface. The detailed description of this step is beyond the scope of this report but the interested reader can refer to Ref. [1], [2] for more information about low thermal budget surface preparation.

1.1 Full-sheet epitaxy

1.1.1 Si growth

Precursors and temperature dependence

The precursors used to grow Si layers are usually H or Cl-based molecules such as SiH₄ (silane), Si₂H₆ (disilane), or SiH₂Cl₂ (dichlorosilane or DCS). Chlorinated chemistries (and in particular DCS+HCl) are often adopted in modern semiconductor processing flows since they allow the epitaxy to be selective. However, as shown in Fig. 1, the growth rate of an epitaxy using DCS is lower compared to H-based precursors (Si₂H₆ and SiH₄), for the same experimental conditions at low temperatures [3], [4]. In contrast, similar growth rates are observed at high temperatures. As a consequence, DCS is not the most suitable precursor for low thermal budget processes ($\leq 600^\circ\text{C}$) as required for 3D sequential integration.

¹ Also referred as Rapid Thermal CVD (RT-CVD).

The Si growth kinetics with SiH_4 and SiH_2Cl_2 exhibits two temperature regimes: at high temperatures ($T > 950^\circ\text{C}$ for SiH_2Cl_2 and $T > 850^\circ\text{C}$ for SiH_4), the growth rate is limited by precursor supply and dissociations (i.e., there is almost no temperature dependence) while at low temperatures, the growth rate is limited by H and/or Cl desorption at the surface and exhibits an Arrhenius temperature dependence [5]. In Ref. [3], the epitaxial growth was carried out using a 300 mm Epsilon 3200 tool from ASM America. Based on the measured growth rates, activation energies of 2.13 eV for SiH_4 and 2.52 eV for SiH_2Cl_2 were reported. Similarly, in Ref. [6] activation energies of 2.17 eV for SiH_4 and 2.30 eV for SiH_2Cl_2 have been reported based on epitaxial growth using a 200 mm Epi Centura tool from Applied Materials.

Similar values were also obtained in the benchmark of two 300 mm RP-CVD tools in Ref. [7]. The growth rate kinetics of Si_2H_6 is more complicated and the low temperature regime (i.e., for $T < 850^\circ\text{C}$) can be decomposed in three different temperature regimes: a growth rate "plateau" between 575°C and 675°C surrounded by two domains with a different activation energy (1.39 eV for $T > 675^\circ\text{C}$ and 2.3 eV for $T < 575^\circ\text{C}$) [3]. The Si growth kinetics in the low temperature regime using precursor mixing ($\text{Si}_2\text{H}_6 + \text{SiH}_2\text{Cl}_2$ and $\text{Si}_2\text{H}_6 + \text{SiH}_4$) has also been investigated in Ref. [4] but results in a reduction of the growth rate compared to pure Si_2H_6 .

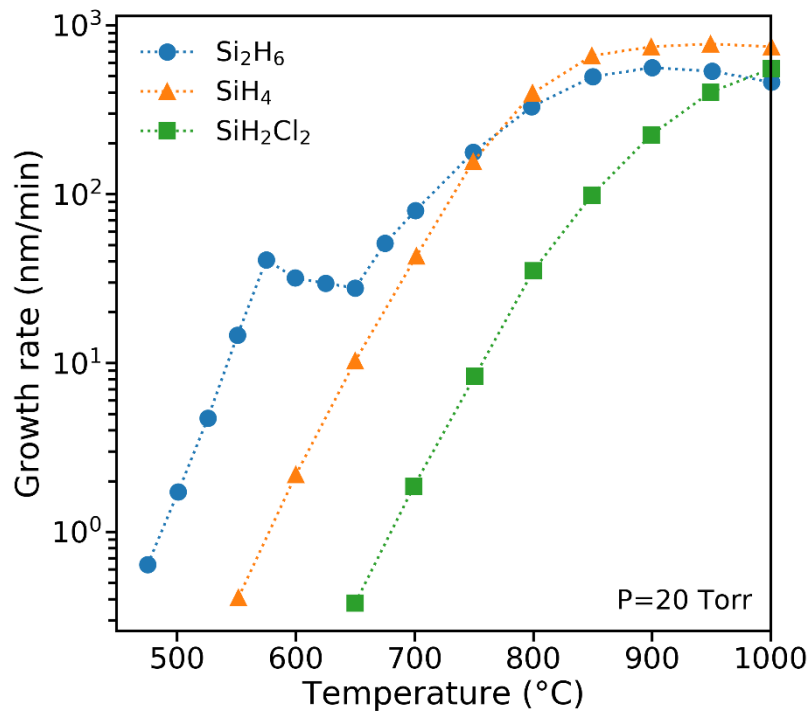


Fig. 1: Silicon growth rate as a function of the temperature for Si_2H_6 , SiH_4 and SiH_2Cl_2 precursors (at 20 Torr) reported in Ref. [3]. The same Si flux was used ($F(\text{SiH}_2\text{Cl}_2)/F(\text{H}_2)=0.012$, $F(\text{SiH}_4)/F(\text{H}_2)=0.012$ and $F(\text{Si}_2\text{H}_6)/F(\text{H}_2)=0.006$).

Orientation dependence

The Si growth rate depends on the substrate orientation and has been studied in detail in Ref. [8] for the case of DCS with H_2 as carrier gas. Fig. 2 shows the growth rate as a function of temperature for (100), (110) and (111) orientations. The Si growth rates on (110) and (111) substrate are systematically lower compared to (100). In the high temperature regime, the growth rate on Si(111) is higher compared to Si(110) while the opposite is true for the low temperature regime.

In the low temperature regime, the growth rate anisotropy can be attributed to (i) the difference in the dangling bond densities in each plane² and (ii) a probably different H desorption rate depending on the surface [8], [9].

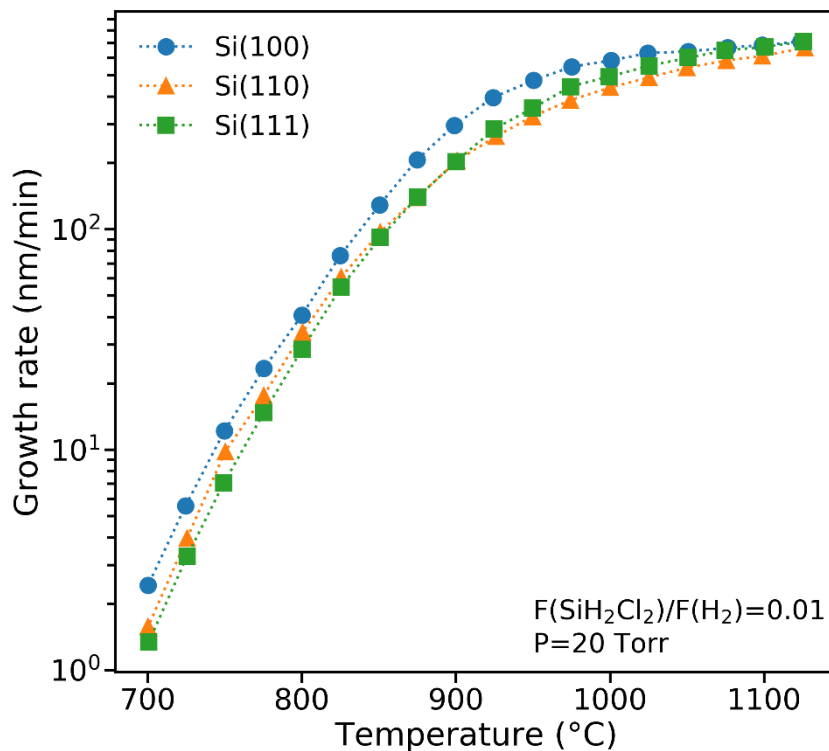


Fig. 2: Silicon growth rate as a function of temperature for {100}, {110} and {111} substrate orientations (at 20 Torr) using a DCS chemistry reported in Ref. [8].

1.1.2 SiGe growth

The growth of SiGe layers requires to add a Ge precursor to the chemistry (in addition to Si precursors), such as GeH_4 (Germane) or Ge_2H_6 (Digermane). An important difference to the case of Si homoepitaxy described in Section 1.1.1 is that SiGe layers grown on Si are biaxially strained due to the lattice parameter mismatch between Si and SiGe. As a consequence, beyond a critical thickness, the formation of misfit dislocations starts to be energetically favorable leading to the plastic relaxation of the layer. The critical thickness for plastic relaxation has been investigated experimentally by many studies. In particular, in Ref. [10], Hartmann *et al.* have studied it in a 200 mm RP-CVD epitaxy tool for Ge concentrations below 50% and temperatures ranging from 550°C to 700°C.

Flow ratio and temperature dependence

Fig. 3 shows experimental SiGe growth rate as a function of the $F(\text{GeH}_4)/F(\text{SiH}_2\text{Cl}_2)$ flow ratio for different temperatures between 550°C and 750°C [3]. The growth rate increases linearly with the flow of GeH_4 due to the catalyzed desorption of H and Cl atoms in presence of Ge atoms. In Ref. [3], the growth rate dependence has also been investigated for $\text{GeH}_4+\text{SiH}_4$ and Si_2H_6 chemistries. The SiGe growth rate has been shown to increase linearly with the GeH_4 flow for Si_2H_6 and super-linearly with SiH_4 . In addition, the Ge content dependence of the

² The dangling bond densities of (110) and (111) surfaces are $1/\sqrt{2}$ and $1/\sqrt{3}$ compared to (100) surface, respectively.

deposited SiGe layer with the $F(\text{GeH}_4)/F(\text{Si precursor})$ flow ratio is almost linear for SiH_4 and parabolic for SiH_2Cl_2 and Si_2H_6 Si precursors [3], [11].

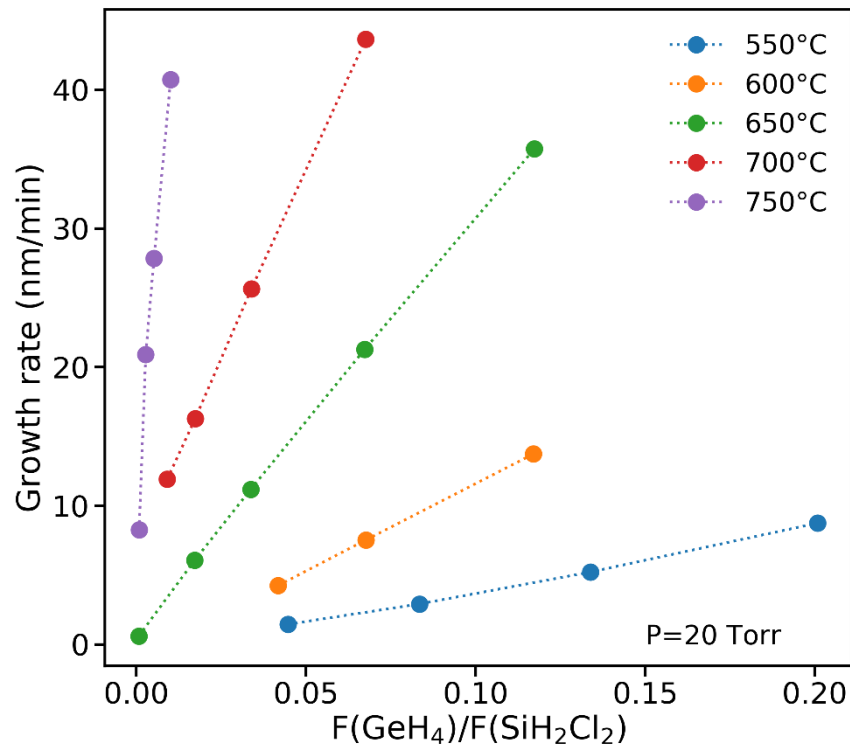


Fig. 3: SiGe growth rate as a function of $F(\text{GeH}_4)/F(\text{SiH}_2\text{Cl}_2)$ ratio. The $F(\text{SiH}_2\text{Cl}_2)/F(\text{H}_2)$ flow ratio was set to 0.003 for $550^\circ\text{C} \leq T \leq 700^\circ\text{C}$ and 0.012 for $T=750^\circ\text{C}$. Data are taken from [3].

Orientation dependence

Fig. 4 shows the SiGe growth rate for layers grown on Si(100), Si(110) and Si(111) as a function of $F(\text{GeH}_4)/F(\text{H}_2)$ flow ratio at fixed process conditions (temperature, pressure and constant $F(\text{SiH}_2\text{Cl}_2)/F(\text{H}_2)$ flow ratio), from Ref. [8]. In the case of (100) surface, the SiGe growth rate increases almost linearly with GeH_4 flow, while for (110) and (111) surfaces it increases sub-linearly, leading to lower growth rates than on Si(100) for high GeH_4 flows. A similar behavior was observed between (100) and (110) growth for difference process conditions in Ref. [2].

For a given set of gaseous flows [8], a decrease of the Ge concentration is observed when switching from (100) to (111) and even more for (110) surfaces.

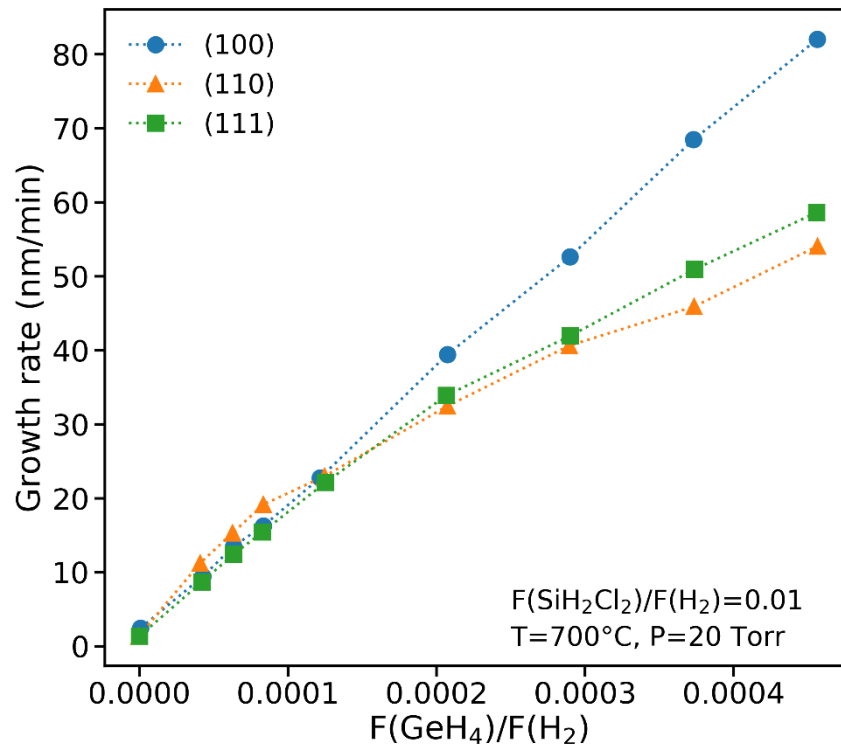


Fig. 4: SiGe growth rate as a function of $F(\text{GeH}_4)/F(\text{H}_2)$ flow ratio. The SiGe layers are grown on Si(100), Si(110) and Si(111) substrates at 700°C and 20 Torr at a constant $F(\text{SiH}_2\text{Cl}_2)/F(\text{H}_2)=0.01$ flow ratio. The data are taken from Ref. [8].

1.1.3 Etching

In Sections 1.11.1.1 and 1.1.2, we focused on the growth of epitaxial layers. However, to achieve selective epitaxy an etchant, usually HCl (Hydrochloric acid), is added to the growth chemistry [12] in the so-called co-flow approach. Alternatively, SEG can also be achieved with a cyclic deposition/etch (CDE) process which has been patented by Bauer *et al.* [13] (see Section 1.2). It should also be pointed out that for low temperatures epitaxies, HCl becomes inefficient and can be replaced by Cl_2 (Chlorine) [14].

Temperature dependence

Similarly, to the CVD growth, the HCl etching exhibits a high temperature and a low temperature regime. This is illustrated in Fig. 5, where etching is achieved with HCl only or HCl+GeH₄ chemistries. In the 1000-1100°C range, the etch rates are almost the same. In contrast, in the low temperature regime the etching rate follows a linear Arrhenius dependence with temperature [15]. The fact to add GeH₄ (usually used to grow SiGe layers, as discussed in Section 1.1.2), allows to boost the low-temperature etch rate by reducing the activation energy from 3.1 eV (i.e. pure HCl) to 1.91 eV [15], [16]. It has indeed be found that the etch rate of SiGe is much faster than for Si [17]–[20].

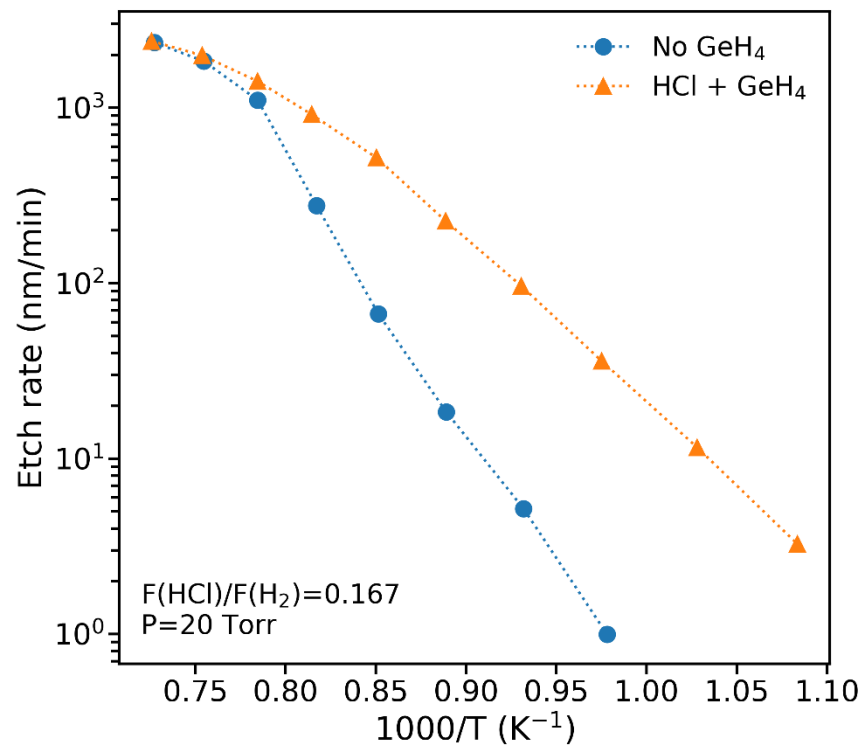


Fig. 5: Arrhenius plot of the etch rate with HCl or HCl+GeH₄ of Si(100) at 20 Torr from Ref. [15]. In the case of HCl+GeH₄, the flow ratio $F(\text{GeH}_4)/F(\text{H}_2)$ was 1.33×10^{-3} .

Orientation dependence

In the high temperature regime ($T > 925^\circ\text{C}$), etch rates using HCl do not depend on surface orientation [20]. In contrast, at lower temperature, the etching rate on (110) surfaces is found to be four times higher than for (100) [2], [20]. Chemical vapor etching has also been studied by Dutartre *et al.* using patterned structures where they managed to extract the etch rate of {111} planes. They found that etching is slower on {111} planes compared to {100} even in the high temperature regime.

1.1.4 In-situ doping: SiGe:B and Si:P

In-situ doping can be achieved by adding precursors containing dopant atoms to the chemistry. In the case of p-type doping, B₂H₆ (diborane) is usually used to form SiGe:B layers while for n-type doping PH₃ (phosphine) is used to grow Si:P layers [16], [21], [22].

SiGe:B

An increase of the SiGe:B growth rate with the B₂H₆ flow is usually observed (keeping other parameters fixed):

- For Si₂H₆+GeH₄+B₂H₆+HCl chemistry (Ref. [21], [23])
- For SiH₂Cl₂+GeH₄+B₂H₆+HCl (Ref. [24])
- For SiH₄+GeH₄+B₂H₆ (Ref. [25])

In the Si₂H₆ and SiH₂Cl₂ cases, the increase of the B₂H₆ flow resulted also in a lowering of the Ge concentration [21], [24]. The concentration of electrically active B is process dependent but can reach values beyond the thermodynamic equilibrium, typically below 10^{19} cm^{-3} for B in

Si [26]. For example, in Ref. [21], the authors developed a SiGe:B process at 450°C where the active B concentration increases linearly with the B₂H₆ flow from 1.8 up to 8.3x10²⁰ cm⁻³. Similar high concentrations were also reported using Ge₂H₆ instead of GeH₄ [27].

Si:P

The low temperature growth kinetics of Si:P exhibits a different behavior when SiH₄ or Si₂H₆ is used as a Si precursor [15]:

- In the case of SiH₄+PH₃, the growth rate at 650°C drops rapidly with the PH₃ flow while the P ion concentration increases almost linearly with F(PH₃)/F(SiH₄) flow ratio and saturates reaching relatively low concentrations (around 2x10¹⁹ cm⁻³) due to P segregation at the surface.
- In the case of Si₂H₆+PH₃, the growth rate at 550°C slightly increases with the PH₃ flow. The P concentration increases linearly with the F(PH₃)/2F(Si₂H₆) flow ratio up to 1.7x10²⁰ cm⁻³. Similar P concentrations around 10²⁰ cm⁻³ were also reported in Si₂H₂Cl₂+PH₃ grown layers at 700°C [28].

Higher P concentrations can be achieved in tensile-strained SiC:P layers. For example, in Ref. [15] P concentrations up to 3.9x10²⁰ cm⁻³ were obtained with a Si₂H₆+SiCH₆+PH₃ chemistry. Very high P activation have also been obtained in Si:P but requiring a post-epitaxy ms laser anneal (see Ref. [29] and references therein).

1.2 Patterned substrates

In most of the technological applications, epitaxy has to be selective on patterned wafers. In the case of advanced CMOS devices, the growth has to be achieved in very small areas ranging between 10 and 40 nm requiring the development of complex CVD processes. In such devices, the growth usually occurs simultaneously on various surface orientations and gives rise to the formation of facets [12], [30]. The apparition of facets results from the growth and etch kinetics anisotropy and is highly dependent on experimental conditions. The main facets usually observed during CVD epitaxy are the {001}, {311} and {111} ones and may coexist in a same growth [12], [31], [32]. For example, in Ref. [12], Si layers was grown at different temperatures in (001) Si trenches using SiH₂Cl₂ and H₂ as a carrier gas. The authors observed the formation of {311} facets at 850°C, no faceting at 750°C and a competition between {311} and {001} growth at 800°C. They also studied the growth on patterned structures made of {111} facets and observed that these facets propagate at 750°C while at 850°C they vanish rapidly giving rise to {311} facets.

In addition, an important phenomenon that take place during SEG is the so-called loading effects that lead to a different growth kinetics between patterned and full-sheet epitaxy [33], [34]. They are caused by to two main contributions: (i) a thermal effect (i.e. thermal fluctuation during the deposition) and (ii) a chemical effect. Loading effects typically lead to variations of the deposited layer thickness and the Ge content in the case of SiGe epitaxy.

In the case of low temperature epitaxy (T<600°C), SEG using a co-flow approach may not be feasible. In this case, it has to be replaced by a cyclic deposition/etch (CDE) process [13]. It consists in depositing a few nm of Si (or SiGe) non-selectively (e.g. Si₂H₆ for Si and Si₂H₆+GeH₄ for SiGe) on patterned wafers giving rise to crystalline layers on active Si or SiGe area and amorphous or polycrystalline layers on dielectrics. Amorphous and polycrystalline materials are then etched selectively using an etching chemistry (e.g. Cl₂ or GeH₄+HCl) and the process is repeated several times in order to achieve the desired thickness. CDE allows to

achieve full selectivity and is particularly well suited for 3D sequential integration where the thermal budget is limited.

2 Modeling review

Lattice kinetic Monte Carlo (LKMC) modeling is a standard approach used to model epitaxial growth of Si, SiGe, and Ge. It has proven able to predict for example faceting and growth rates [35]–[39]. Sentaurus Process of Synopsys [40] is the gold standard for TCAD process simulations in the industry, and the implemented LKMC models for epitaxial growth are considered as state-of-the-art. Different model classes are available in Sentaurus Process, with different levels of complexity [38]:

- A simple, but effective, model based on the work of Martin-Bragado and Moroz [35]. It is a quantitative physically based atomistic model built up by several orientation-dependent deposition rates. The orientation dependence is set through the prefactors of the deposition rates.
- A model based on the work of Chen *et al.* [36], where the rates are governed by neighbor-binding interactions up to the third nearest neighbor. In this model, the anisotropic growth is a result of the position of the new atoms on the surface with respect to its neighbors.

The implemented model based on Chen *et al.* [36] is the most complex of the available model classes in Sentaurus Process [40], and contains the most features [38]. The default implementation is used as the starting point for the MUNDFAB project. Section 2.1 contains an evaluation of that model. A large range of gases for the precursor is already implemented in Sentaurus Process [40]. The ones available are possibly sufficient for the MUNDFAB project. It is nevertheless possible to implement further gases if necessary. A potential drawback of the models in Sentaurus Process is that neither reactions in the gas phase nor effects related to the reactor geometry are considered [38].

Whether further extensions of these models are necessary to reach the goals of the MUNDFAB project will be evaluated during the course of the project. Should it then not be able to implement them in Sentaurus Process, we will use the LKMC tool MulSKIPS [41], [42] which was already shown to be suitable for the modeling of the formation of twin and stacking-fault defects. MulSKIPS is open source and was developed by one of the partners (CNR) for epitaxial growth of cubic SiC (3C-SiC) [41], [42]. However, the framework needs further adaptation before it can be applied to the epitaxial growth of Si, SiGe, and Ge. More information about MulSKIPS is given in Section 2.2.

An alternative implementation to Sentaurus Process [40] was presented by Balbuena and Martin-Bragado [39]. They used the LKMC module of the MMonCa simulation toolkit [43] to implement models for epitaxial growth of silicon using a precursor with SiH₄ and H₂ as carrier gas. The model is based on transition state theory, and the reaction rates are based on the work of Chen *et al.* [36].

2.1 Simulations of full-sheet epitaxy with Sentaurus Process

For confidentiality reasons, it is not possible to disclose details of the implemented models in Sentaurus Process [40] including the reaction paths and parameter values that have not been published. However, the models can still be evaluated based on a comparison of simulation results and experimental data. Here, the simulation results are obtained using the most

advanced model, `Coordinations.Reactions`, based on the work of Chen *et al.* [36], with default parameters from Advanced Calibration (Q-2019.12) [40]. It should also be mentioned that Sentaurus Process [40] offers many different options for the simulations, the options used here are summarized in Fig. 6.

A few examples for Si and SiGe have been chosen to highlight where the model can be improved. At this point, in-situ doping is not included since some issues already appear for cases without doping. These need to be handled before addressing the more complex case of in-situ doping.

```
math coord.ucs
SetAtomistic
AdvancedCalibration

pdbSet LKMC Epitaxy.Model      Coordinations.Reactions
pdbSet KMC Epitaxy             true
pdbSet KMC Simplify.Geometry  1e-4
pdbSet KMC Decade              10
pdbSet KMC InitOutputTime     0.1

pdbSet LKMC Epitaxy.Cleanup           false
SetInterfaceInjectionLKMC             false
pdbSet LKMC Epitaxy.Deposit.Complex   false
pdbSet LKMC Diffusion                  false
pdbSet LKMC Epitaxy.Desorption.Flux   false
pdbSet LKMC Dangling.Bond.Model       false
pdbSet LKMC Diffusion                  true

## Only in the case of SiGe and Ge epitaxy:
LKMC_SiGe_Epitaxy
pdbSet LKMC Lattice.Density.Correction 1
KMC_SiGe_and_Stress_Effect             1 0
```

Fig. 6: Settings used for the simulations using Sentaurus Process (version Q-2019.12 [40]). Note that slightly different options are used in the case of SiGe and Ge.

2.1.1 Simulation of silicon epitaxial growth

Comparison between precursors

In Fig. 7, the data presented in Fig. 1 are shown again together with the simulation results. While the agreement is generally very well, the simulation results are not able to predict the plateau region around 600 °C visible in the data for Si_2H_6 . The growth rate at high temperatures is overestimated by the simulation results, and the slight drop around 1000 °C is not captured. The increase in the growth rate in the simulation results at around 500 °C is artificial; it is related to very rough surfaces. The SiH_2Cl_2 and SiH_4 data are captured quite well by the simulation results. However, there is an increasing offset in the case of SiH_2Cl_2 at lower temperatures, where the simulation results overestimate the growth rate.

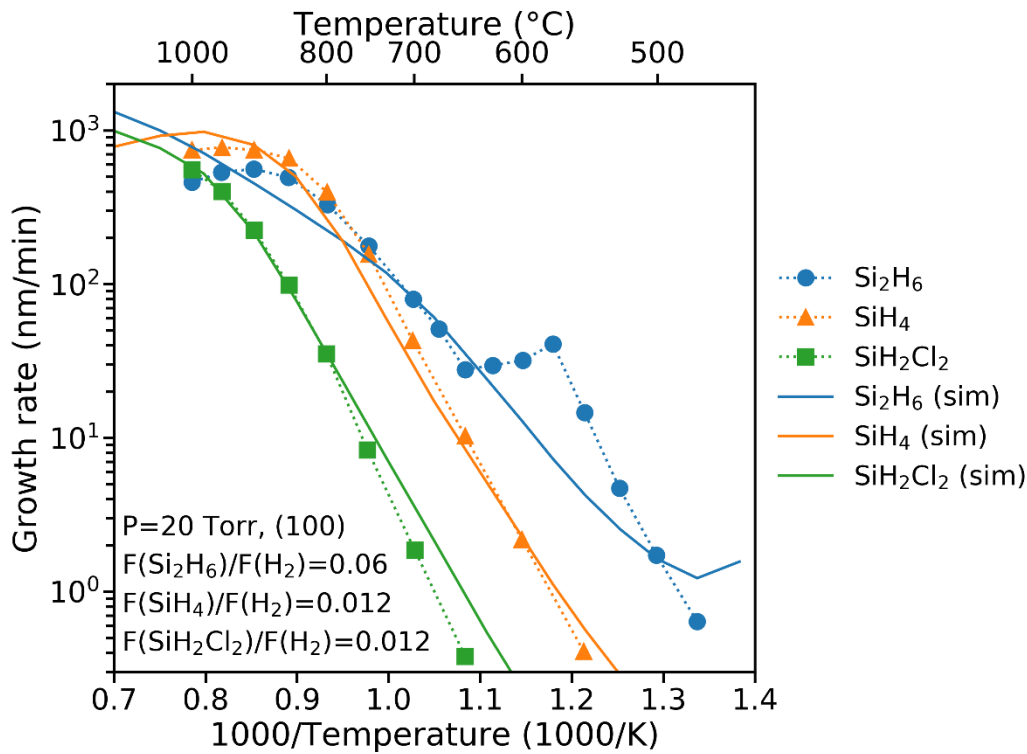


Fig. 7: Silicon growth rate as a function of the temperature for Si_2H_6 , SiH_4 and SiH_2Cl_2 precursors (at 20 Torr). The data were reported in Ref. [4]. The simulations were carried out with Sentaurus Process (Q-2019.12) and the settings listed in Fig. 6.

Impact of anisotropy

As shown in the experimental section, the wafer orientation has an influence on the growth rate. Two examples of simulation results are shown in Fig. 8 and Fig. 9, using SiH_2Cl_2 for the precursor. In Fig. 8, the growth rates are shown as a function of the temperature for different surface orientations (100), (110), and (111). Overall, the data are again captured quite well by the simulation results. However, at lower temperatures, the growth rates are overestimated for all orientations. The growth rate is underestimated for (111)-oriented wafers at higher temperatures. In Fig. 9, the growth rates are shown as a function of the flow ratio of SiH_2Cl_2 at a temperature of 750 °C for different surface orientations (100), (110), and (111). The data trends are captured quite well by the simulation results.

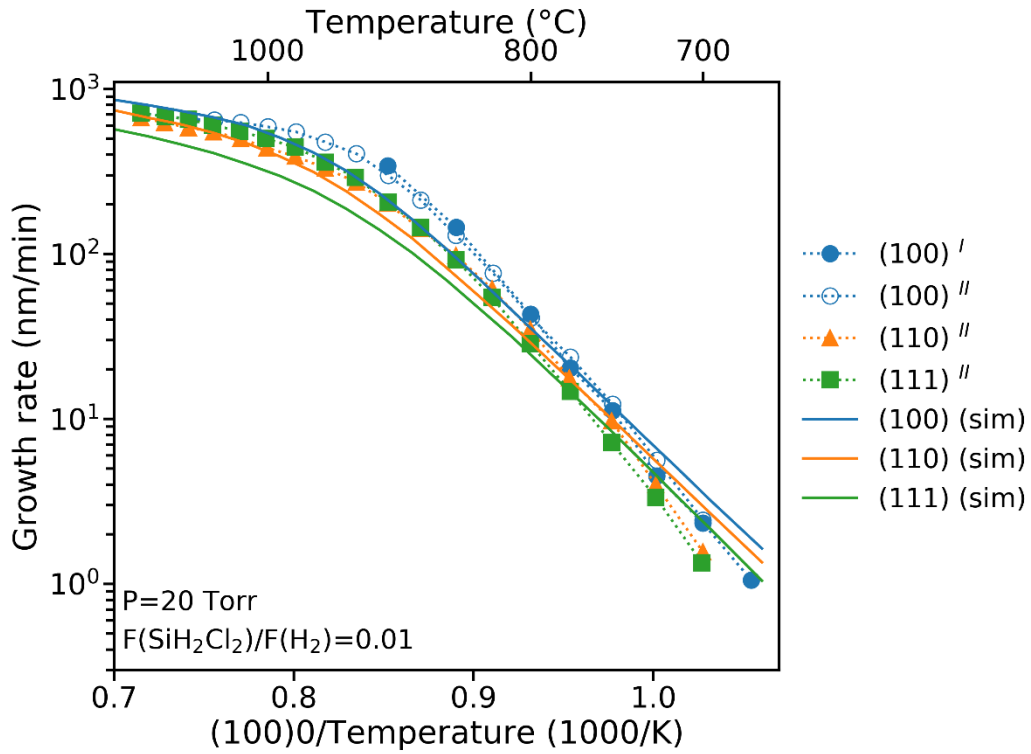


Fig. 8: Silicon growth rate as a function of the temperature for a precursor with SiH₂Cl₂ (at 20 Torr). The I-data were reported in Ref. [22] and the II-data were reported in Ref. [8]. The simulations were carried out with Sentaurus Process (Q-2019.12) and the settings listed in Fig. 6.

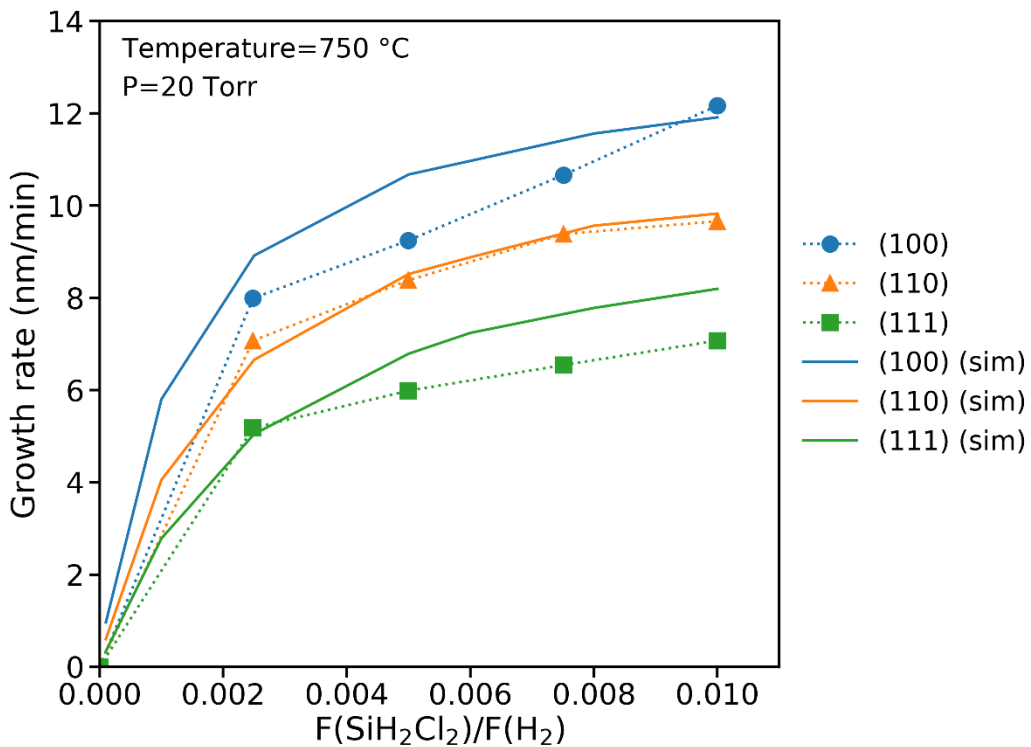


Fig. 9: Silicon growth rate as a function of the flow ratio F(SiH₂Cl₂)/F(H₂) (at 20 Torr and a temperature of 750 °C). The data were reported in Ref. [8]. The simulations were carried out with Sentaurus Process (Q-2019.12) and the settings listed in Fig. 6.

Impact of adding HCl

Another important aspect of the modelling is to capture the effects of adding HCl to the precursor. Two examples of simulation results are shown in Fig. 10 and Fig. 11, using a precursor with SiH_2Cl_2 and HCl. In Fig. 10, the growth rates are shown as a function of the temperature for different flow ratios, and in Fig. 11, the growth rates are shown as a function of the flow ratio of HCl at a temperature of 750 °C for (100)-, (110)-, and (111)-oriented wafers. Overall, the fit to the data is considerably worse compared to the case without HCl. In Fig. 10, the higher the flow ratio of HCl, the more the growth rate is overestimated by the simulation results. The same trend can be recognized in Fig. 11 for all orientations.

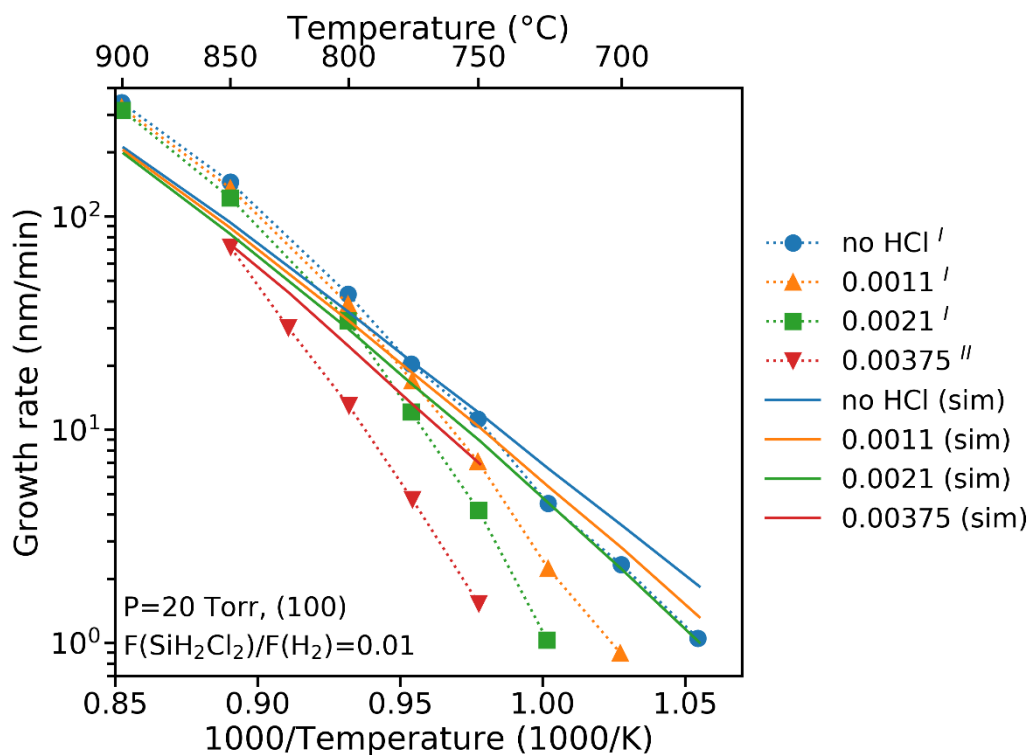


Fig. 10: Silicon growth rate as a function of the temperature for a precursor with SiH_2Cl_2 and HCl (at 20 Torr). The I-data were reported in Ref. [22] and the II-data were reported in Ref.[8]. The simulations were carried out with Sentaurus Process (Q-2019.12) and the settings listed in Fig. 6.

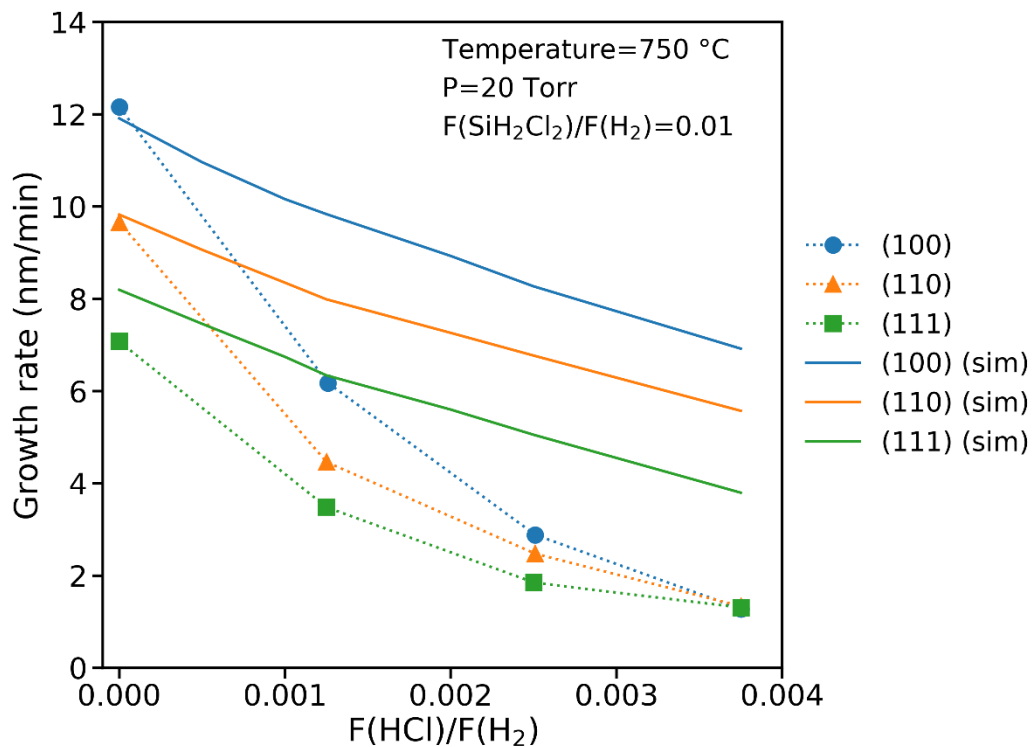


Fig. 11: Silicon growth rate as a function of the flow ratio $F(\text{HCl})/F(\text{H}_2)$ (at 20 Torr and a temperature of 750 °C). The data were reported in Ref.[8]. The simulations were carried out with Sentaurus Process (Q-2019.12) and the settings listed in Fig. 6.

2.1.2 Simulation of epitaxial growth of SiGe

Impact of the flow ratio of GeH_4

To investigate how well the model captures the growth of SiGe several experiments were simulated. A representative example of simulation results is shown in Fig. 12, using SiH_2Cl_2 and GeH_4 precursors. The growth rates (right) and germanium concentrations (left) are shown as a function of the flow ratio of GeH_4 at different temperatures. The simulation results do not capture the trend of the growth rate data. The growth rate is overestimated for higher flow ratios of GeH_4 at all temperatures. The germanium concentration is better captured, but it is overestimated at 550 °C, and underestimated at 700 °C.

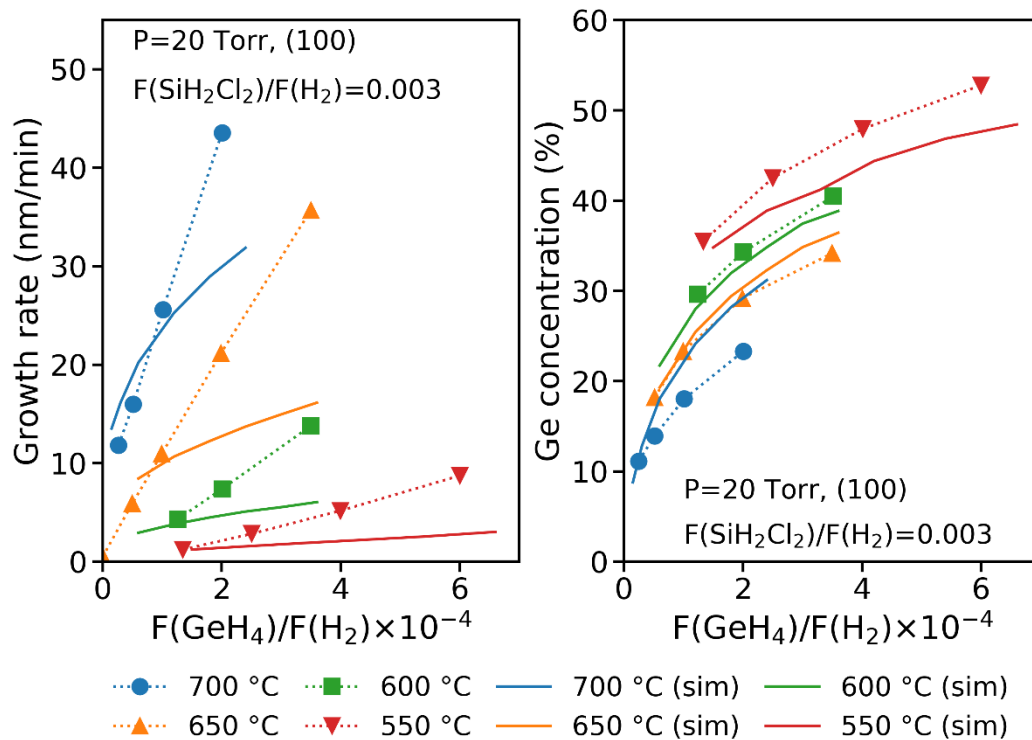


Fig. 12: SiGe growth rate (to the right) and germanium concentration (to the left) as a function of the flow ratio $F(\text{GeH}_4)/F(\text{H}_2)$ for a precursor with SiH_2Cl_2 and GeH_4 (at 20 Torr). The data were reported in Ref. [4]. The simulations were carried out with Sentaurus Process (Q-2019.12) and the settings listed in Fig. 6. Note that the additional options for SiGe were used.

Impact of adding HCl

The effect of adding HCl to the precursor for the growth of SiGe was also investigated. An example of simulation results is shown in Fig. 13, using a precursor with SiH_2Cl_2 , GeH_4 , and HCl. The growth rates (right) and germanium concentrations (left) are shown as a function of the flow ratio of GeH_4 with and without added HCl. The simulation results do not capture the trend of the growth rate data. The growth rate is overestimated for higher flow ratios of GeH_4 at all temperatures, as in Fig. 12. The data indicate that the germanium concentration is higher in the case of added HCl, which is not captured by the simulations.

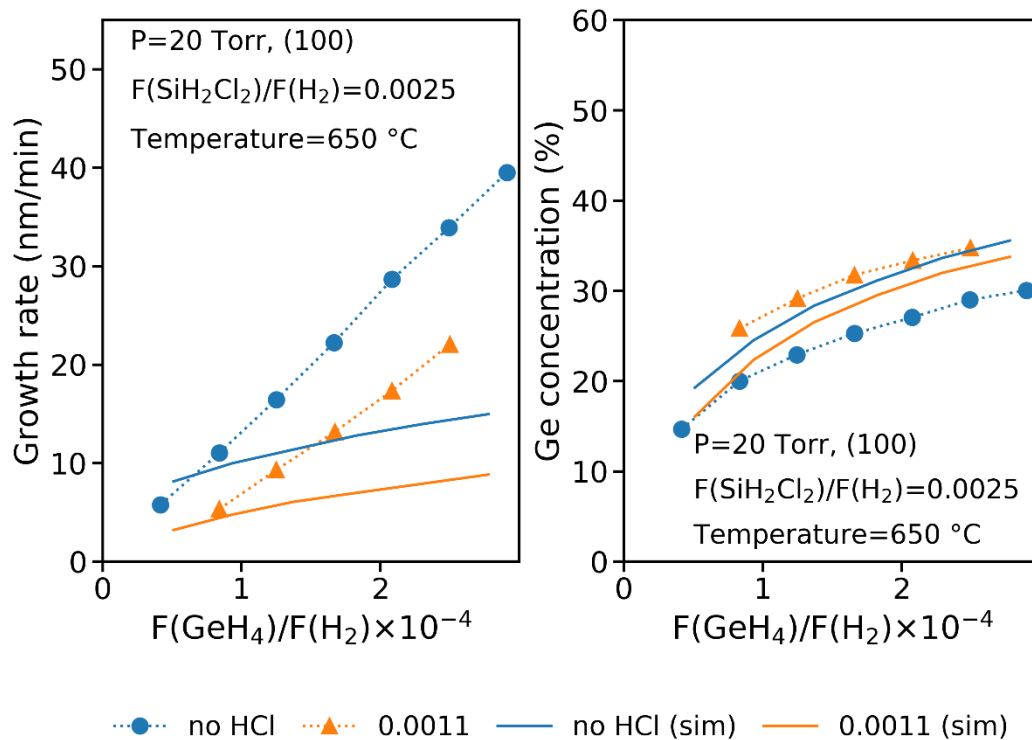


Fig. 13: SiGe growth rate (to the right) and germanium concentration (to the left) as a function of the flow ratio $F(\text{GeH}_4)/F(\text{H}_2)$ for a precursor with SiH_2Cl_2 , GeH_4 , and HCl (at 20 Torr and a temperature of 650 °C). The data were reported in Ref. [4], [22]. The simulations were carried out with Sentaurus Process (Q-2019.12) and the settings listed in Fig. 6. Note that the additional options for SiGe were used.

2.2 Epitaxy simulation with MulSKIPS

MulSKIPS is a Kinetic Monte Carlo super-Lattice code, designed to study at an atomic resolution the growth kinetics of elements, alloys and compounds characterized by the sp^3 bond symmetry. Formalization and implementation details of the code are discussed in Ref. [41]. The code is open source and it is distributing according a GNU type license³.

Deposition and evaporation of the substrate atoms are the active Monte Carlo events, driving the stochastic evolution. In MulSKIPS a dense super-lattice, where the original lattice of the ideal crystal is a sub-lattice of the super-lattice itself, accommodate correctly a large class of defective configurations [41], [42], [44], [45]. This feature makes the code unique in the range of lattice Kinetic Monte Carlo codes currently available. Indeed, the code is able to simulate the evolution of both point-like and extended defects, like stacking faults of different symmetries, antiphase boundaries and grain boundaries. Moreover, MulSKIPS can simulate also the morphology evolution during the growth e.g.: the epitaxial growth or etching of flat, structured, or patterned substrates, as well as nanoparticles of various shapes. In the case of surfaces, periodic boundary conditions are applied in the planes orthogonal to the growth direction.

In order to be reliably applied to a given material, configuration-dependent parameters have to be calibrated using a more fundamental approach, or by means of a fitting procedure with ad-hoc experiments performed in controlled conditions. To increase the predictivity power of the stochastic evolution, input frequencies for the local transitions involving atoms bonded X to the evolving surface/interfaces can be set by means of a sequential multi-scale approach. In the

³ See code web page at <https://github.com/giuseppefiscaro/mulskips> where user manual and regression tests for developer can be also downloaded.

latter case, *ab initio* energetics at a density functional theory level fix temperature-dependent Monte Carlo frequencies.

Since surface transitions imply bond breaking, we assume that the related evaporation frequencies follow Arrhenius-type functions of the generalized binding energies $E\{\Sigma_{loc}(X,t)\}$ for the X detachment

$$\nu(X,t) = \nu_0(T) \times \exp\left[\frac{-E\{\Sigma_{loc}(X,t)\}}{kT}\right] \quad (1)$$

We note that the frequency in Eq. 1 depends on the local atomic configurations $\Sigma_{loc}(X,t)$ around atom X before the transition, which we classify by means of the number one/two/three and type of sp^3 bonds in the first-neighbor shell. Arrhenius pre-factors $\nu_0(T)$ can be set with partial pressures at equilibrium in the gas phase during the substrate sublimation. This approach guarantees that the method is also calibrated to the temperature-dependent sublimation kinetics of the material in equilibrium with its gas components.

Deposition frequencies depend on the experimental controlled growth conditions implemented in the CVD or physical vapor deposition (PVD) chambers. In MulSKIPS modelling approach, these frequencies are again configuration dependent. They reproduce the average rate of atoms attached/released at the substrate interface independently from the particular reactions' mechanisms involving atomic or molecular components in the vapor phase. As a consequence, the Monte Carlo events in MulSKIPS correspond to real exchange of atomic species for the case of PVD; whilst for the CVD process they effectively describe the path of multiple reactions occurring in the vapor phase or at the solid-vapor phase boundary which leads to addition/removal of a substrate atom. Usually CVD deposition frequencies can be calibrated to reproduce experimental time-dependent epitaxial growth profiles in CVD growth processes on structured substrates and impurity markers. Another possibility is to couple MulSKIPS with zero-dimensional or three-dimensional simulators of the reaction chamber to properly evaluate the deposition kinetics.

Comparing the Sentaurus Process and MulSKIPS formalisms and respective nomenclature, we can finally conclude that: a) the "Deposition" event in MulSKIPS describes a sequence of "Absorption" and "Surface Reaction" events of Sentaurus Process; the "Evaporation" event in MulSKIPS describes a sequence of "Etching" + "Desorption" events of Sentaurus Process.

As a representative case of study, we report a MulSKIPS simulation for the epitaxial growth of 3C-SiC substrates exposing the (001) surface (the z axis of the Cartesian system lies along the [001] direction) [42]. Ref. [42] reports details for the calibration strategy as well as a comprehensive frame of the MulSKIPS capabilities. A cubic simulation box with a side of 740.8 Å was set. Considering the super-lattice description, the box contained $\sim 8 \times 10^9$ sites. We started the MulSKIPS run from a 3C-SiC slab with a thickness of 137.8 Å. The initial active KMC particles lying at the (001) surface consisted of 51200 under-coordinated atoms. The kinetic Monte Carlo simulation produced a vacancy point defect density of $7 \times 10^{17} \text{ cm}^{-3}$ (eventual bulk annihilation of vacancies is not included in this case). Considering a growth velocity of 1 $\mu\text{m}/\text{hour}$ we obtain a flux rate for vacancy generation of $2 \times 10^{10} \text{ cm}^{-2} \text{ s}^{-1}$. In many replica of equivalent simulated growths (from the stochastic point of view), no generation of extended defects has been observed, demonstrating that this growth direction is rather robust against extended defect formation. Surface is flat (atomic scale roughness) and this is a usual characteristic of the implemented formalism.

Extended defects generation can be studied by MulSKIPS when initial substrate preparation boosts their formation (e.g. presence of faceting, nanostructures or non-ideal bonding like

antiphase boundaries). This feature is not obtained by an “ad-hoc” labelling of the substrate lattice points but it emerges as reconfiguration of the atoms location and bounding in the super lattice description of the defective configuration. In Fig. 15 and example of multiple stacking fault generation is reported for a simulation performed with exact same conditions of that reported in Fig. 14 apart for the presence of and antiphase boundary in the initial substrate. Again, the many-replica analysis confirms this result.

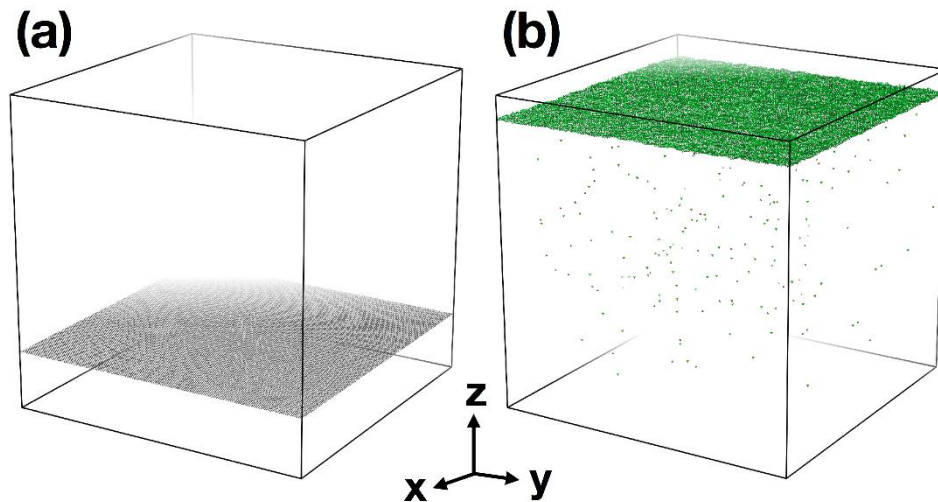


Fig. 14: Epitaxial growth of a 3C-SiC substrate exposing the (001) surface (the z axis of the Cartesian system lies along the [001] direction).

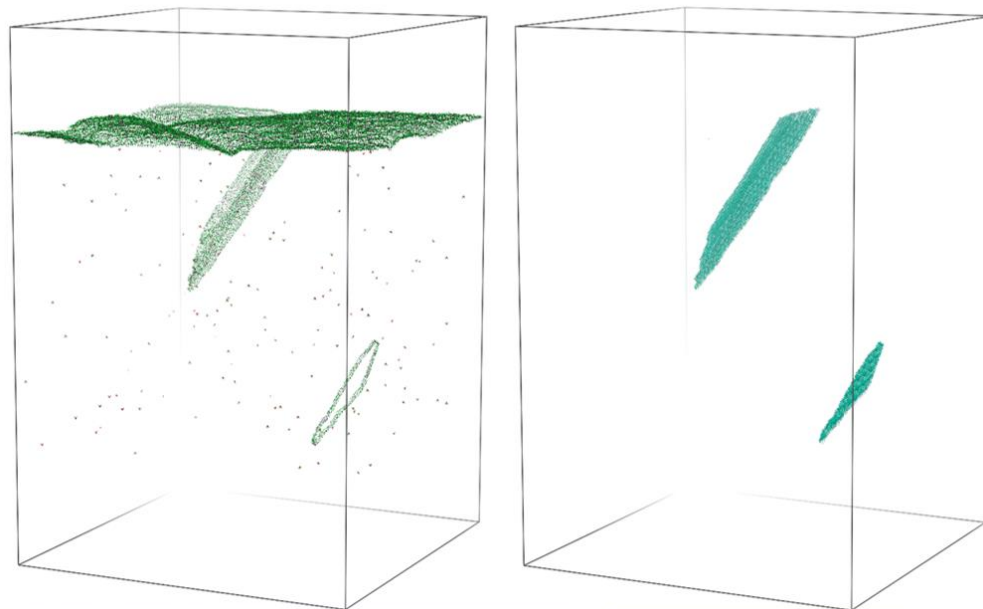


Fig. 15: Multiple stacking fault defect generation during an epitaxial growth of a 3C-SiC substrate exposing the (001) surface and presenting a preexisting anti phase boundary bulk defect.

Conclusions

In this deliverable, a review of the state of the art of CVD epitaxy has been presented from an experimental and modeling perspective. Experimentally, the growth (and etch) kinetics highly

depends on process parameters such as the precursors and their partial pressure, the deposition temperature and pressure, or the carrier gas. Many experimental data including variations of different process conditions are available in the literature and can be used to calibrate or validate the models developed in the frame of the MUNDFAB project.

Although the model implemented in Sentaurus Process can describe a large part of the available experimental data, there is room for improvement. It is necessary to further improve the model to capture effects for the temperatures and precursors relevant for the MUNDFAB project, especially in the case of added HCl and for SiGe.

Finally, the LKMC model implemented in MulSKIPS to simulated PVD epitaxy of 3C-SiC has been presented and possible extension of the actual model to simulate CVD epitaxy has been proposed. This could be particularly well suited for the simulation of extended defects during the epitaxy of strained layers.

References

- [1] A. Abbadie, J. M. Hartmann, P. Holliger, M. N. Séméria, P. Besson, and P. Gentile, "Low thermal budget surface preparation of Si and SiGe," *Applied Surface Science*, vol. 225, no. 1, pp. 256–266, Mar. 2004, doi: 10.1016/j.apsusc.2003.10.018.
- [2] V. Destefanis, J. M. Hartmann, M. Hopstaken, V. Delaye, and D. Bensahel, "Low-thermal surface preparation, HCl etch and Si/SiGe selective epitaxy on (110) silicon surfaces," *Semicond. Sci. Technol.*, vol. 23, no. 10, p. 105018, Sep. 2008, doi: 10.1088/0268-1242/23/10/105018.
- [3] J. M. Hartmann, V. Benevent, J. F. Damlencourt, and T. Billon, "A benchmarking of silane, disilane and dichlorosilane for the low temperature growth of group IV layers," *Thin Solid Films*, vol. 520, no. 8, pp. 3185–3189, Feb. 2012, doi: 10.1016/j.tsf.2011.10.164.
- [4] J. M. Hartmann, "Impact of Si precursor mixing on the low temperature growth kinetics of Si and SiGe," *Semicond. Sci. Technol.*, vol. 33, no. 10, p. 104002, Aug. 2018, doi: 10.1088/1361-6641/aad8d2.
- [5] J.-M. Hartmann, "Epitaxy of Strained Si/Si_{1-x}Ge_x Heterostructures," in *Silicon Technologies*, John Wiley & Sons, Ltd, 2013, pp. 209–331.
- [6] J. M. Hartmann *et al.*, "Growth kinetics of Si on fullsheet, patterned and silicon-on-insulator substrates," *Journal of Crystal Growth*, vol. 257, no. 1, pp. 19–30, Sep. 2003, doi: 10.1016/S0022-0248(03)01380-0.
- [7] J.-M. Hartmann, V. Mazzocchi, F. Pierre, and J.-P. Barnes, "A Benchmark of 300mm RP-CVD Chambers for the Low Temperature Epitaxy of Si and SiGe," *ECS Trans.*, vol. 86, no. 7, p. 219, Jul. 2018, doi: 10.1149/08607.0219ecst.
- [8] J. M. Hartmann, M. Burdin, G. Rolland, and T. Billon, "Growth kinetics of Si and SiGe on Si(100), Si(110) and Si(111) surfaces," *Journal of Crystal Growth*, vol. 294, no. 2, pp. 288–295, Sep. 2006, doi: 10.1016/j.jcrysgro.2006.06.043.
- [9] C. Pribat and D. Dutartre, "Anisotropy effects during non-selective epitaxial growth of Si and SiGe materials," *Journal of Crystal Growth*, vol. 334, no. 1, pp. 138–145, Nov. 2011, doi: 10.1016/j.jcrysgro.2011.08.021.
- [10] J. M. Hartmann, A. Abbadie, and S. Favier, "Critical thickness for plastic relaxation of SiGe on Si(001) revisited," *Journal of Applied Physics*, vol. 110, no. 8, p. 083529, Oct. 2011, doi: 10.1063/1.3656989.
- [11] J. M. Hartmann *et al.*, "SiGe growth kinetics and doping in reduced pressure-chemical vapor deposition," *Journal of Crystal Growth*, vol. 236, no. 1, pp. 10–20, Mar. 2002, doi: 10.1016/S0022-0248(01)02085-1.
- [12] D. Dutartre, A. Talbot, and N. Loubet, "Facet Propagation in Si and SiGe Epitaxy or Etching," *ECS Trans.*, vol. 3, no. 7, p. 473, Oct. 2006, doi: 10.1149/1.2355845.
- [13] M. Bauer *et al.*, "Selective deposition of silicon-containing films," US7816236B2, Oct. 19, 2010.

-
- [14] A. Hikavy, C. Porret, E. Rosseel, A. Milenin, and R. Loo, "Application of Cl_2 for low temperature etch and epitaxy," *Semicond. Sci. Technol.*, vol. 34, no. 7, p. 074003, Jun. 2019, doi: 10.1088/1361-6641/aafc93.
- [15] J. M. Hartmann, V. Benevent, J. P. Barnes, M. Veillerot, and C. Deguet, "Disilane-based cyclic deposition/etch of Si, Si:P and $\text{Si}_{1-y}\text{C}_y$:P layers: I. The elementary process steps," *Semicond. Sci. Technol.*, vol. 28, no. 2, p. 025017, Jan. 2013, doi: 10.1088/0268-1242/28/2/025017.
- [16] J. M. Hartmann and M. Veillerot, "HCl + GeH_4 etching for the low temperature cyclic deposition/etch of Si, Si:P, tensile-Si:P and $\text{SiGe}(\text{:B})$," *Semicond. Sci. Technol.*, vol. 35, no. 1, p. 015015, Nov. 2019, doi: 10.1088/1361-6641/ab52ec.
- [17] Y. Bogumilowicz, J. M. Hartmann, R. Truche, Y. Campidelli, G. Rolland, and T. Billon, "Chemical vapour etching of Si, SiGe and Ge with HCl applications to the formation of thin relaxed SiGe buffers and to the revelation of threading dislocations," *Semicond. Sci. Technol.*, vol. 20, no. 2, pp. 127–134, Dec. 2004, doi: 10.1088/0268-1242/20/2/004.
- [18] Y. Bogumilowicz, J. M. Hartmann, J. M. Fabri, and T. Billon, "Selective chemical vapour etching of $\text{Si}_{1-x}\text{Ge}_x$ versus Si with gaseous HCl," *Semicond. Sci. Technol.*, vol. 21, no. 12, pp. 1668–1674, Oct. 2006, doi: 10.1088/0268-1242/21/12/028.
- [19] V. Destefanis, J. M. Hartmann, S. Borel, and D. Bensahel, "High pressure in situ HCl etching of $\text{Si}_{1-x}\text{Ge}_x$ versus Si for advanced devices," *Semicond. Sci. Technol.*, vol. 23, no. 10, p. 105019, Sep. 2008, doi: 10.1088/0268-1242/23/10/105019.
- [20] J. M. Hartmann, V. Destefanis, G. Rabillé, and S. Monfray, "HCl selective etching of SiGe versus Si in stacks grown on (110)," *Semicond. Sci. Technol.*, vol. 25, no. 10, p. 105009, Sep. 2010, doi: 10.1088/0268-1242/25/10/105009.
- [21] J. Aubin, J. M. Hartmann, M. Veillerot, Z. Essa, and B. Sermage, "Very low temperature (450 °C) selective epitaxial growth of heavily in situ boron-doped SiGe layers," *Semicond. Sci. Technol.*, vol. 30, no. 11, p. 115006, Oct. 2015, doi: 10.1088/0268-1242/30/11/115006.
- [22] J. M. Hartmann *et al.*, "Selective epitaxial growth of boron- and phosphorus-doped Si and SiGe for raised sources and drains," *Journal of Crystal Growth*, vol. 264, no. 1, pp. 36–47, Mar. 2004, doi: 10.1016/j.jcrysgro.2003.12.055.
- [23] J. M. Hartmann *et al.*, "Very Low Temperature (Cyclic) Deposition/Etch of In Situ Boron-Doped SiGe Raised Sources and Drains," *ECS J. Solid State Sci. Technol.*, vol. 3, no. 11, p. P382, Sep. 2014, doi: 10.1149/2.0161411jss.
- [24] J. M. Hartmann, F. Gonzatti, F. Fillot, and T. Billon, "Growth kinetics and boron doping of very high Ge content SiGe for source/drain engineering," *Journal of Crystal Growth*, vol. 310, no. 1, pp. 62–70, Jan. 2008, doi: 10.1016/j.jcrysgro.2007.10.003.
- [25] J. Hållstedt, A. Parent, M. Östling, and H. H. Radamson, "Incorporation of boron in SiGe(C) epitaxial layers grown by reduced pressure chemical vapor deposition," *Materials Science in Semiconductor Processing*, vol. 8, no. 1, pp. 97–101, Feb. 2005, doi: 10.1016/j.mssp.2004.09.074.
- [26] P. Pichler, *Intrinsic Point Defects, Impurities, and Their Diffusion in Silicon*. Wien: Springer-Verlag, 2004.
- [27] J.-M. Hartmann, J. Aubin, and J.-P. Barnes, "A Benchmark of Germane and Digermane for the Low Temperature Growth of Intrinsic and Heavily in-situ Boron-Doped SiGe," *ECS Trans.*, vol. 75, no. 8, p. 281, Aug. 2016, doi: 10.1149/07508.0281ecst.
- [28] J. M. Hartmann, J. Aubin, S. Barraud, and M. P. Samson, "Atmospheric Pressure Selective Epitaxial Growth of Heavily In Situ Phosphorous-Doped Si(:C) Raised Sources and Drains," *ECS J. Solid State Sci. Technol.*, vol. 6, no. 1, p. P52, Dec. 2016, doi: 10.1149/2.0211701jss.
- [29] E. Rosseel *et al.*, "(Invited) Selective Epitaxial Growth of High-P Si:P for Source/Drain Formation in Advanced Si nFETs," *ECS Trans.*, vol. 75, no. 8, p. 347, Aug. 2016, doi: 10.1149/07508.0347ecst.
- [30] D. Dutartre, B. Seiss, Y. Campidelli, D. Pellissier-Tanon, D. Barge, and R. Pantel, "Faceting and nanostructure effects in Si and SiGe epitaxy," *Thin Solid Films*, vol. 520, no. 8, pp. 3163–3169, Feb. 2012, doi: 10.1016/j.tsf.2011.10.115.
-

- [31] A. Talbot, J. Arcamone, C. Fellous, F. Deleglise, and D. Dutartre, "Investigation of Facet Formation in RTCVD Si/SiGe Selective Epitaxy," presented at the The Electrochemical Society 206th Meeting, 2004.
- [32] N. Loubet *et al.*, "Raised S/D for Advanced Planar MOSFET devices: Challenges and Applications for the 20nm Node and Beyond," presented at the International Conference on Solid State Devices and Materials, Tokyo, 2010.
- [33] C. Reichel *et al.*, "SiGe channels for V_T control of high-k metal gate transistors for 32nm complementary metal oxide semiconductor technology and beyond," *Thin Solid Films*, vol. 520, no. 8, pp. 3170–3174, Feb. 2012, doi: 10.1016/j.tsf.2011.10.093.
- [34] C. Fellous, F. Romagna, and D. Dutartre, "Thermal and chemical loading effects in non selective Si/SiGe epitaxy," *Materials Science and Engineering: B*, vol. 89, no. 1, pp. 323–327, Feb. 2002, doi: 10.1016/S0921-5107(01)00773-5.
- [35] I. Martin-Bragado and V. Moroz, "Modeling of {311} facets using a lattice kinetic Monte Carlo three-dimensional model for selective epitaxial growth of silicon," *Appl. Phys. Lett.*, vol. 98, no. 15, p. 153111, Apr. 2011, doi: 10.1063/1.3580771.
- [36] R. Chen, W. Choi, A. Schmidt, K.-H. Lee, and Y. Park, "A new kinetic lattice Monte Carlo modeling framework for the source-drain selective epitaxial growth process," in *2013 International Conference on Simulation of Semiconductor Processes and Devices (SISPAD)*, Sep. 2013, pp. 9–12, doi: 10.1109/SISPAD.2013.6650561.
- [37] S.-Y. Lee *et al.*, "Atomistic simulation flow for source-drain epitaxy and contact formation processes of advanced logic devices," in *2016 International Conference on Simulation of Semiconductor Processes and Devices (SISPAD)*, Sep. 2016, pp. 101–104, doi: 10.1109/SISPAD.2016.7605158.
- [38] N. Zographos, C. Zechner, I. Martin-Bragado, K. Lee, and Y.-S. Oh, "Multiscale modeling of doping processes in advanced semiconductor devices," *Materials Science in Semiconductor Processing*, vol. 62, pp. 49–61, May 2017, doi: 10.1016/j.mssp.2016.10.037.
- [39] J. P. Balbuena and I. Martin-Bragado, "Lattice kinetic Monte Carlo simulation of epitaxial growth of silicon thin films in H_2/SiH_4 chemical vapor deposition systems," *Thin Solid Films*, vol. 634, pp. 121–133, Jul. 2017, doi: 10.1016/j.tsf.2017.05.013.
- [40] "Sentaurus Process of Synopsys with Advanced Calibration (version Q-2019-12)." Synopsys, 2019.
- [41] A. La Magna *et al.*, "Simulation of the Growth Kinetics in Group IV Compound Semiconductors," *physica status solidi (a)*, vol. 216, no. 10, p. 1800597, 2019, doi: 10.1002/pssa.201800597.
- [42] G. Fisicaro *et al.*, "Genesis and evolution of extended defects: The role of evolving interface instabilities in cubic SiC," *Applied Physics Reviews*, vol. 7, no. 2, p. 021402, Apr. 2020, doi: 10.1063/1.5132300.
- [43] I. Martin-Bragado, A. Rivera, G. Valles, J. L. Gomez-Selles, and M. J. Caturla, "MMonCa: An Object Kinetic Monte Carlo simulator for damage irradiation evolution and defect diffusion," *Computer Physics Communications*, vol. 184, no. 12, pp. 2703–2710, Dec. 2013, doi: 10.1016/j.cpc.2013.07.011.
- [44] M. Camarda, A. La Magna, and F. La Via, "A kinetic Monte Carlo method on super-lattices for the study of the defect formation in the growth of close packed structures," *Journal of Computational Physics*, vol. 227, no. 2, pp. 1075–1093, Dec. 2007, doi: 10.1016/j.jcp.2007.08.036.
- [45] M. M. Bunea and S. T. Dunham, "Monte Carlo study of vacancy-mediated impurity diffusion in silicon," *Phys. Rev. B*, vol. 61, no. 4, pp. R2397–R2400, Jan. 2000, doi: 10.1103/PhysRevB.61.R2397.